Triphenylamine/Tetracyanobutadiene-Based π-Conjugated Push–Pull Molecules End-Capped with Arene Platforms

Simon Marques, Pablo; Castan, Jose Maria Andres; Raul, Benedito A. L.; Londi, Giacomo; Ramirez, Ivan; Pshenichnikov, Maxim S.; Beljonne, David; Walzer, Karsten; Blais, Martin; Allain, Magali

Link to publication in University of Groningen/UMCG research database

Chemistry–A European Journal

Full Paper
doi.org/10.1002/chem.202002810

Check for updates

Europe
European Chemical
Societies Publishing

▌Donor–Acceptor Systems │*Hot Paper*│

Triphenylamine/Tetracyanobutadiene-Based π-Conjugated Push–Pull Molecules End-Capped with Arene Platforms: Synthesis, Photophysics, and Photovoltaic Response

Pablo Simón Marqués[+],[a] José María Andrés Castán,[a] Benedito A. L. Raul[+],[b] Giacomo Londi[+],[c] Ivan Ramirez,[d] Maxim S. Pshenichnikov,*[b] David Beljonne,*[c] Karsten Walzer,[d] Martin Blais,[a] Magali Allain,[a] Clément Cabanetos,[a] and Philippe Blanchard*[a]

Abstract: π-Conjugated push–pull molecules based on triphenylamine and 1,1,4,4-tetracyanobuta-1,3-diene (TCBD) have been functionalized with different terminal arene units. In solution, these highly TCBD-twisted systems showed a strong internal charge transfer band in the visible spectrum and no detectable photoluminescence (PL). Photophysical and theoretical investigations revealed very short singlet excited state deactivation time of ≈ 10 ps resulting from significant conformational changes of the TCBD-arene moiety upon photoexcitation, opening a pathway for non-radiative decay. The PL was recovered in vacuum-processed films or when the molecules were dispersed in a PMMA matrix leading to a significant increase of the excited state deactivation time. As shown by cyclic voltammetry, these molecules can act as electron donors compared to C_{60}. Hence, vacuum-processed planar heterojunction organic solar cells were fabricated leading to a maximum power conversion efficiency of ca. 1.9% which decreases with the increase of the arene size.

Introduction

Small donor–acceptor conjugated push–pull molecules (D-π-A) represent an outstanding class of materials due to their inherent low-energy intramolecular charge-transfer (ICT) band in the visible to the near infrared (NIR) region, with in some cases, aggregation induced emission (AIE) or thermally-activated delay fluorescence (TADF) properties. As a result, they have found various electronic and optoelectronic applications in nonlinear optics (NLO),[1,2] organic light-emitting diodes (OLEDs),[3] bio-imaging,[4] dye-sensitized solar cells (DSSCs)[5,6] and organic solar cells (OSCs).[6] In particular, related dipolar systems based on arylamines as electron-donating D building block which provide good hole-transporting properties,[7] have been extensively investigated for the preparation of efficient donor materials for organic photovoltaics (OPV).[6,8] Depending on their structure, this type of relatively simple molecules can combine good solubility in common solvents and evaporability allowing the fabrication of highly performing single-junction organic solar cells (OSCs) either by solution-processing[9] or vacuum deposition.[10] Recently, multi-junction OSCs based on arylamine-based D-π-A push–pull molecules with power conversion efficiency (*PCE*) exceeding 10% have been reported, highlighting the potential of this class of molecular donors.[11]

Following the pioneer article of J. Roncali on the use of a push–pull molecule for OPV,[12] namely the star-shaped triphenylamine (TPA) compound **TPA(T-DCV)₃**, some of us have recently shown that the linear, simpler and more easily accessible triphenylamine-thiophene-dicyanovinyl molecule, namely **TPA-T-DCV**, exhibits comparable and even superior photovoltaic (PV) properties when combined with C_{60} or its soluble analogue [6,6]-phenyl-C_{61}-butyric acid methyl ester ($PC_{61}BM$) as acceptors (Scheme 1).[13] Starting from **TPA-T-DCV**, minimal structural changes of: i) the TPA unit aiming at improving the hole transport properties,[14] ii) the π-spacer toward extended electronic delocalization[13d] and iii) the strength of the electron-withdrawing group A,[13b] led to enhanced PV performance. Recently, the substitution of the hydrogen atom of the DCV

[a] *P. Simón Marqués,[+] J. M. A. Castán, M. Blais, M. Allain, Dr. C. Cabanetos, Dr. P. Blanchard*
MOLTECH-Anjou, UMR CNRS 6200
UNIV Angers, SFR MATRIX
2 bd Lavoisier, 49045 ANGERS Cedex (France)
E-mail: philippe.blanchard@univ-angers.fr

[b] *B. A. L. Raul,[+] Prof. Dr. M. S. Pshenichnikov*
Zernike Institute for Advanced Materials, University of Groningen
Nijenborgh 4, 9747 AG, Groningen (The Netherlands)
E-mail: m.s.pchenitchnikov@rug.nl

[c] *G. Londi,[+] Dr. D. Beljonne*
Laboratory for Chemistry of Novel Materials
University of Mons, Place du Parc, 20, 7000 Mons (Belgium)
E-mail: david.beljonne@umons.ac.be

[d] *Dr. I. Ramirez, Dr. K. Walzer*
HELIATEK GmbH, Treidlerstraße 3, 01139 Dresden (Germany)

[+] *These authors contributed equally to this work.*

📖 *Supporting information and the ORCID identification number(s) for the author(s) of this article can be found under:*
https://doi.org/10.1002/chem.202002810.

Chemistry–A European Journal

Full Paper
doi.org/10.1002/chem.202002810

Chemistry Europe
European Chemical
Societies Publishing
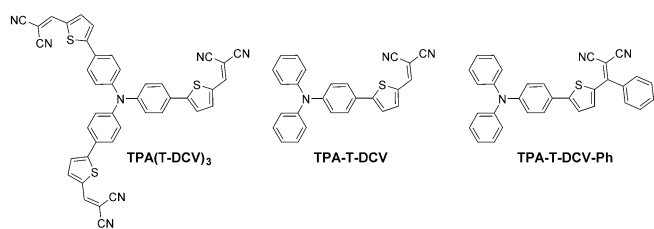
Scheme 1. Previously described DCV-based push–pull molecules as donors for OPV.

Scheme 2. Chemical structure of **TPA-T-1**, and the new phenyl (**Ph-1**), naphthyl (**Napht-1**), pyrenyl (**Pyr-1**)-functionalized TCBD-based push–pull molecules.

group by a phenyl ring gave rise to the new thermally stable derivative **TPA-T-DCV-Ph** that showed an unusual long exciton diffusion length (> 25 nm) and was used in vacuum-processed bulk heterojunction (BHJ) OSCs with C_{70} leading to a *PCE* higher than 5%.[15]

In this context, the "click"-type [2+2] cycloaddition-retroelectrocyclization (CA-RE) reaction between an electron-rich alkyne and electron-deficient olefin, suc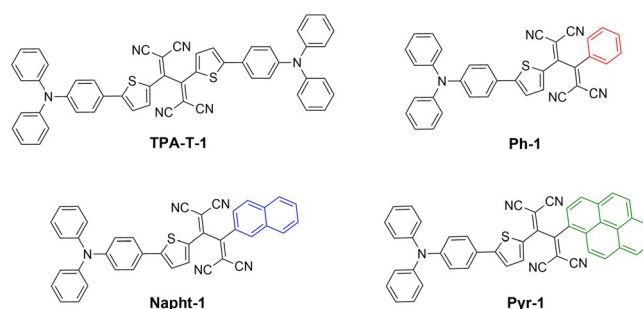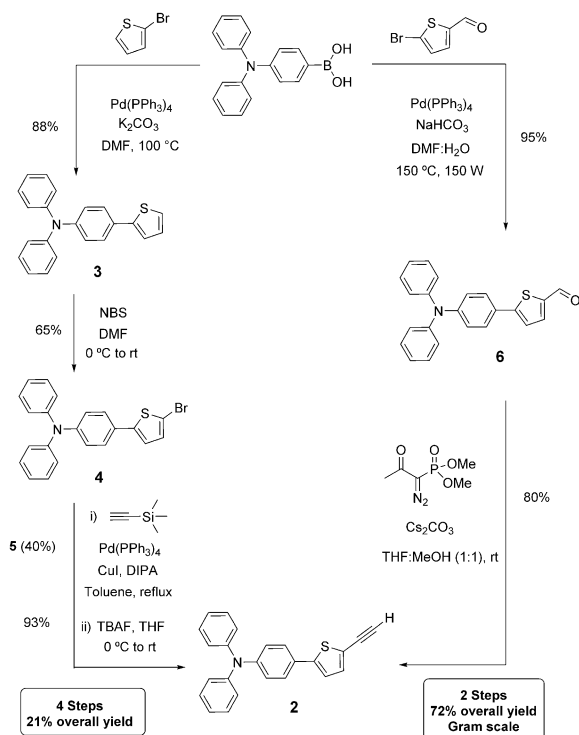h as tetracyanoethylene (TCNE) leading to 1,1,4,4-tetracyanobuta-1,3-diene (TCBD) derivatives,[16] has attracted our interest. This efficient reaction performed in the absence of catalyst under mild conditions allows for the introduction of TCBD, a strong electron-accepting block (A), which is particularly convenient for the synthesis of thermally stable D-π-A push–pull conjugated molecules endowed with interesting optical properties. As initially reported for NLO applications,[17] the presence of TCBD in D-π-A push–pull chromophores induces a non-planar conformation improving the solubility and leading to an intense and low-energy ICT band in the visible spectrum.[18] These results triggered the synthesis and photophysical investigations of various electro- and photoactive D-A multicomponent systems[19] while some devices for all-optical switching have been fabricated.[20] On the other hand, as expected for strongly-coupled donor-acceptor systems, the photoluminescence (PL) of TCBD-based push–pull chromophores is in general extremely weak, and in some cases even not measurable in solution due to ultrafast (≈1 ps) radiationless deactivation of the first singlet excited state.[21] This process can compete with charge separation, which is expected at the interface between the donor and acceptor materials in OSCs, hence limiting the interest of TCBD derivatives for OPV. However, while the self-assembly of a bis-TCBD derivative into vesicles or nanotubes led to aggregation-induced emission properties as early reported in 2008,[22] a very recent work on pyrene- and perylene-functionalized TCBD derivatives shows that whereas PL is not observed in solution, it is indeed detectable in the solid state, with emission reaching the NIR region up to 1350 nm, which opens interesting perspectives for bio-imaging.[23]

Earlier, we described the synthesis and electronic properties of symmetrical and unsymmetrical D-π-A-π-D molecules using TCBD as the accepting central core and oligothienyl-TPA chains as donor blocks, and reported for the first time the use of a TCBD derivative, namely **TPA-T-1**, as donor material for OPV leading to a *PCE* of ca. 1.1% (Scheme 2).[24] Since then, other TCBD-derived push–pull molecular donors and extended dicyanoquinodimethane (DCNQ) analogues have been de-

scribed in the literature for the fabrication of solution-processed BHJ OSCs with $PC_{61}BM$ or $PC_{71}BM$ leading to *PCE*s between ca. 3% and 6%.[25] In addition, due to the strong electron-withdrawing character of TCBD and DCNQ, different push–pull molecules have also been successfully used as non-fullerene acceptors (NFAs) and combined with donor polymers in BHJ OSCs giving rise to promising *PCE*s up to 7%.[26] It must be noted that different molecules combining TPA and TCBD have been also investigated for their third-order nonlinear optical properties.[27]

In this work, new unsymmetrical TPA-derived D-π-A push–pull molecules based on TCBD have been functionalized with a terminal phenyl (**Ph-1**), a 2-naphthyl (**Napht-1**) or a 1-pyrenyl (**Pyr-1**) unit (Scheme 2). The larger arene blocks are expected to provide additional optical properties and develop π–π intermolecular interactions in the solid state as already observed in pyrene-functionalized TCBD derivatives[28] and small molecules for efficient BHJ OSCs.[29] X-ray diffraction on single crystals has given us insights into the structure and intermolecular interactions in the solid state of the titled compounds. Their electrochemical and optical properties have been characterized by cyclic voltammetry, steady state absorption, (time-resolved) PL measurements, and ultrafast pump-probe experiments in various environments. The latter results have been rationalized on the basis of theoretical calculations and finally discussed with the PV performance of these new molecular donors.

Results and Discussion

Synthesis

The synthesis of the TCBD-based push–pull molecules is based on the free alkyne compound **2**, which can be engaged in a Sonogashira coupling with various monohalogenated arene derivatives affording aryl-end capped alkynes **7** for subsequent CA-RE reaction with TCNE (Scheme 4). As described in Scheme 3, compound **2** was prepared following two different routes. First, a Suzuki coupling between the commercial (4-(diphenylamino)phenyl)boronic acid and 2-bromothiophene gave derivative **3** in good yields. As previously reported,[24] the selective monobromination of **3** in the presence of NBS led to **4** which was subjected to a Sonogashira coupling with trimethyl-

Chemistry–A European Journal

| Full Paper
doi.org/10.1002/chem.202002810

**Chemistry
Europe**
European Chemical
Societies Publishing

**Scheme 3.** Optimization of the synthesis of **2**.

silylacetylene. The silyl group of the intermediate compound **5** was deprotected affording **2** in 93% yield. Thus, compound **2** was obtained in four steps in a 21% overall yield starting from the triphenylamine-derived boronic acid.

A significantly optimized route to **2** was developed in two steps in a 72% overall yield. After a Suzuki coupling between (4-(diphenylamino)phenyl)boronic acid and 5-bromothiophene-2-carbaldehyde,[30] the resulting aldehyde **6** was subjected to a Seyferth–Gilbert homologation using the Ohira–Bestmann reagent affording the desired free alkyne **2**. In addition, this two-step reaction sequence could be carried out on a gram scale.

The first attempts of coupling **2** and iodobenzene under classical Sonogashira conditions in the presence of Cu^I failed affording essentially the dialkyne product resulting from a Glaser homocoupling of **2**. In order to prevent this undesired reaction, a copper-free Sonogashira reaction was used.[31] After optimization, the AsPh$_3$/Pd$_2$(dba)$_3$ catalyst system in the presence of diisopropylamine (DIPA) resulted in the highest yields. Thus, compound **2** reacted with the commercially available iodobenzene, 2-bromonaphthalene or 1-iodopyrene leading to unsymmetrical alkyne derivatives **Ph-7**, **Napht-7** or **Pyr-7**, respectively, in moderate to good yields (Scheme 4). Subsequent reaction with TCNE in refluxing dichloromethane gave the target compounds **Ph-1**, **Napht-1** and **Pyr-1** in quantitative yields.

Crystalline structure of Napht-1

Unlike **Ph-1** and **Pyr-1**, single crystals were successfully grown by slow evaporation of a solution of **Napht-1** in a mixture of
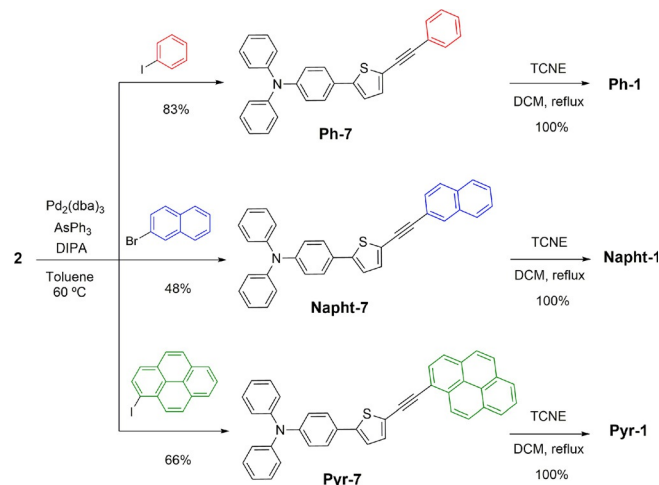
Scheme 4. Synthesis of target compounds **Ph-1**, **Napht-1** and **Pyr-1**.

chloroform and petroleum ether and analyzed by X-ray diffraction. **Napht-1** crystallizes in the cubic $Fd\bar{3}c$ space group with one independent molecule. The phenyl-thiophene-dicyanovinyl (Ph-T-DCV) backbone adopts a quasi-planar conformation with a slight curvature and a DCV unit exhibiting a *s-cis* conformation relative to the neighboring thiophene ring as usually observed (Figure 1).[13b, 32] The two outermost phenyl rings of the TPA unit are out of the aforementioned plane, one of them showing two disordered positions with a 65/35 occupancy rate.

More importantly, the TCBD moiety is highly twisted with a significant dihedral angle of 77° between the two dicyanovinyl groups (Figure 1, bottom), as already reported for other TCBD derivatives,[16a] while the two planes defined by the naphthalene unit and the phenyl-thiophene segment, respectively, are nearly perpendicular (88°) (Figure S29).
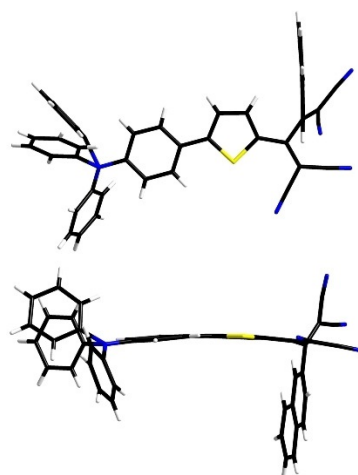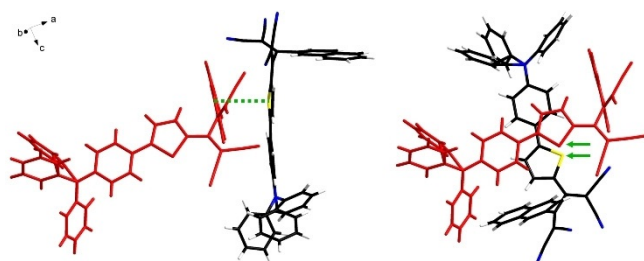

Figure 1. Two different views showing the molecular structure of **Napht-1** obtained from X-ray diffraction of a single crystal. Note that one of the external phenyl ring of TPA adopts two disordered positions with a 65/35 occupancy rate.

Chemistry–A European Journal

Full Paper
doi.org/10.1002/chem.202002810

Chemistry Europe
European Chemical
Societies Publishing

The examination of intermolecular interactions between one selected molecule and their neighbors does not evidence π–π interactions between two slipped planar naphthalene units. However, short intermolecular distances can be found despite the sterically hindered structure of **Napht-1** resulting from the presence of the twisted TCBD. For example, Figure 2 (left) shows that the naphthyl plane of the molecule represented in red, adopts a quasi-parallel (with a deviation angle of only 16°) face-to-face arrangement with the thiophene ring of a neighboring molecule, the intermolecular distance between the sulfur atom and the naphthyl plan being of 3.52 Å. In addition, as shown in Figure 2 (right), the planes defined by the Ph-T-DCV backbone of the two closest neighboring molecules are quasi parallel with a 5° deviation only and separated by a short average distance of 3.27 Å, while the main axes of these two Ph-T-DCV backbones roughly adopt a relative perpendicular orientation. Interestingly, the intermolecular S···S distance of 3.51 Å between the sulfur atoms of each thiophene ring of these two plans is smaller than the sum of the van der Waals radium of two sulfur atoms (3.60 Å) in agreement with the existence of S···S intermolecular interactions.

It is worth noting also that the unit cell of **Napht-1** contains 192 molecules within a volume of 172515 Å³ (Figure S31), which is a rare example of giant organic cubic cells.[33]


Figure 2. Views showing the same selected molecule of **Napht-1** in red and one different neighboring molecule highlighting possible intermolecular interactions between a naphthyl unit and thiophene ring (left) and two quasi parallel planes defined by Ph-T-DCV segments perpendicularly oriented with a short S···S intermolecular distance (3.51 Å) (right).

Electrochemical properties

The electrochemical properties of **Ph-1**, **Napht-1** and **Pyr-1** were investigated by cyclic voltammetry in CH_2Cl_2 in the presence of 0.1 M of Bu_4NPF_6 as supporting electrolyte (Table 1). The cyclic voltammogram (CV) of each compounds was recorded between −1.20 V and +0.70 V vs. Fc/Fc^+ (Figure 3). Both molecules showed one reversible oxidation peak at $E_{pa} = +0.66$ V which could be assigned to the formation of a radical cation localized on the TPA-thiophene branch as previously observed in the **TPA-T-1** reference compound ($E_{pa} = +0.65$ V).[24] When scanning toward negative potentials, the CVs of **Ph-1** and **Napht-1** showed two successive one-electron reversible reduction waves peaking at −0.87 V (E_{pc}^1) and −1.15 V (E_{pc}^2) associated to the reduction of the acceptor TCBD moiety. The first reduction wave of **Pyr-1** was subjected to a positive shift of E_{pc}^1 (−0.77 V) suggesting a stronger electron-accepting char-

Table 1. Cyclic voltammetry data of **Ph-1**, **Napht-1**, **Pyr-1** and reference **TPA-T-1** (Conditions: 1 mM in 0.10 M Bu_4NPF_6/CH_2Cl_2, scan rate 100 mV s⁻¹, Pt working electrode, potentials are expressed vs. Fc/Fc^+)

Compound	E_{pa} [V]	E_{pc}^1 [V]	E_{pc}^2 [V]	E_{HOMO}[a] [eV]	E_{LUMO}[b] [eV]	ΔE^{elec} [eV]
TPA-T-1[23]	0.65	−0.95	−1.11	−5.35	−3.95	1.40
Ph-1	0.66	−0.87	−1.15	−5.41	−3.98	1.43
Napht-1	0.66	−0.87	−1.15	−5.41	−3.98	1.43
Pyr-1	0.66	−0.77	−1.15	−5.41	−4.07	1.33

[a] E_{HOMO} (eV) $= -(E_{ox(onset)}$ vs. $Fc/Fc^+ + 4.8)$. [b] E_{LUMO} (eV) $= -(E_{red(onset)}$ vs. $Fc/Fc^+ + 4.8)$.[34]
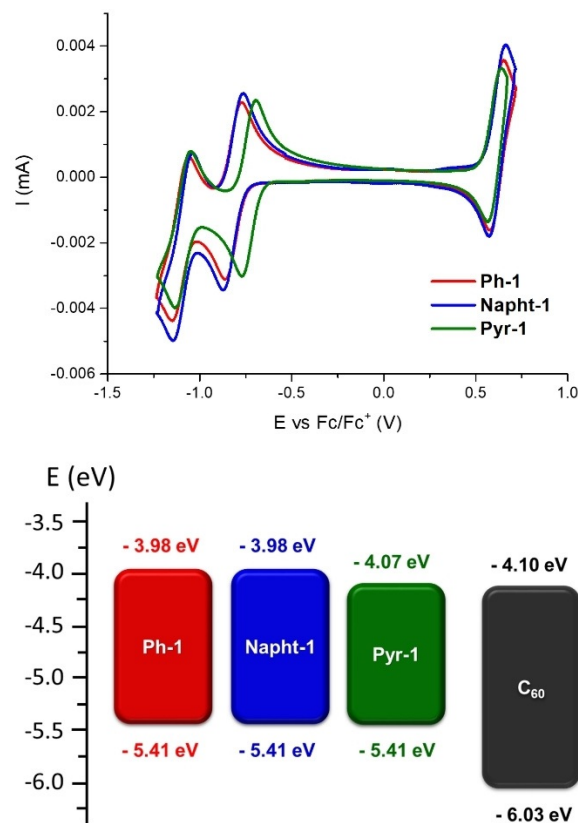
Figure 3. Top: CVs of **Ph-1**, **Napht-1** and **Pyr-1**, 1 mM in 0.10 M Bu_4NPF_6/CH_2Cl_2, scan rate 100 mV s⁻¹, Pt working electrode. Bottom: Energy diagram showing the HOMO and LUMO energy values estimated from CV.

acter of the pyrene unit. Thus, the replacement of one strong electron-donating TPA-T segment in **TPA-T-1** (E_{pc}^1 of −0.95 V) by benzene or extended polycyclic aromatic hydrocarbons induces a positive shift of the first reduction potential peak in agreement with the increased electron-withdrawing character of the later.

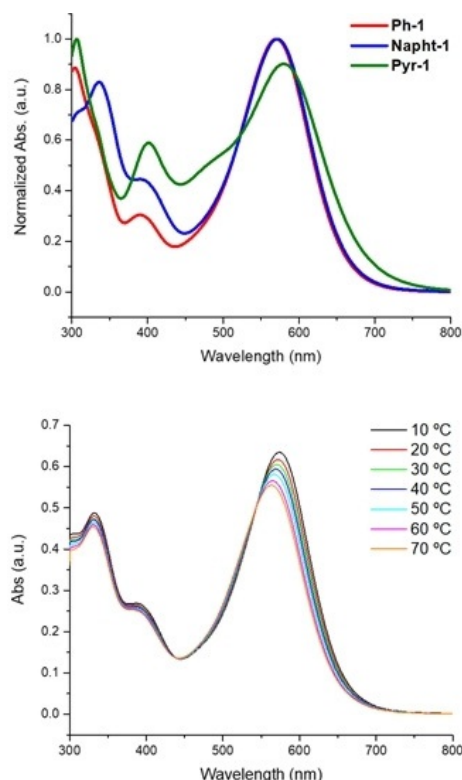The HOMO and LUMO energy levels were estimated from the onsets of the first oxidation and reduction waves giving an electrochemical gap ΔE^{elec} of ca. 1.3–1.4 eV. The HOMO energy level was not affected by the arene substitution for all target molecules (−5.41 eV) suggesting that the HOMO orbital is mainly located on the TPA-thiophene branch of the molecules. In addition, although remaining compatible with a photoin-

Chemistry–A European Journal

Full Paper
doi.org/10.1002/chem.202002810

Chemistry Europe
European Chemical
Societies Publishing

duced electron transfer to C_{60} ($E_{LUMO} = -4.10$ eV)[35] for photovoltaic applications, the LUMO energy level of **Pyr-1** is deeper (-4.07 eV) than those of **Ph-1** and **Napht-1** at -3.98 eV (Figure 3, bottom).

Optical properties

The optical properties of **Ph-1**, **Napht-1** and **Pyr-1** have been analyzed by UV-vis spectroscopy in diluted CH_2Cl_2 solution (ca. 1×10^{-5} M) and as thin-film on glass (Figure 4, Table 2). Their UV-vis spectra show three main absorption bands, with maxima between 305 and 330 nm and between 350 and 450 nm, the last broad and intense one being centered at 571 nm for **Ph-1** and **Napht-1** and redshifted to 580 nm for **Pyr-1**. This latter low-energy broad and intense band can be assigned to an internal charge transfer (ICT) from the electron-donating TPA moiety to the electron-withdrawing TCBD group as observed in **TPA-T-1**, although in this case the corresponding molecular extinction ε is higher due to the presence of two push–pull systems. Theoretical calculations confirmed that the broad low-energy band resulting from the combination of a HOMO → LUMO and a HOMO → LUMO+1 transitions was associated with a strong ICT character (see theoretical calculations section).

In the case of **Pyr-1**, the presence of a shoulder at ca. 480 nm was attributed to an ICT from pyrene to the TCBD moiety in agreement with theoretical calculations and as previously reported for a TCBD-substituted pyrene exhibiting a similar charge transfer band at 483 nm (Figure 4, top).[28a]

The UV-vis spectra of **Ph-1**, **Napht-1** and **Pyr-1** spun cast on glass-sheets from a chloroform solution are slightly broaden and ca. 25 nm redshifted in agreement with the existence of electronic intermolecular interactions in the solid state (Table 2, Figure S32). Optical band gaps (E_g^{opt}) of 1.70, 1.71 and 1.65 eV were estimated from the absorption edges at low energy reaching the NIR region, respectively, values which are close to that of **TPA-T-1** (1.70 eV)[24] (Figure S33) and of interest for photovoltaic conversion.

Additionally, temperature-dependent UV-vis measurements between 10 and 70 °C were performed in chlorobenzene (ca. 1×10^{-5} M) for **Napht-1** (Figure 4, bottom) and **Pyr-1** (Figure S34). For both, the absence of new additional bands at low temperature suggests no aggregation in solution, which may be prevented by the non-planar twisted TCBD central unit, in agreement with X-ray data. Nonetheless, the absorption maximum simply shifted gradually to higher energy when raising the temperature. This could be attributed to the gradual increase of the molecular twisting of the TCBD unit already existing in the crystalline structure. This thermally-induced conformational disorder decreases the effective conjugation and moves the absorption maximum to higher energies.

Figure 4. UV-vis spectra of **Ph-1**, **Napht-1** and **Pyr-1** ca. 10^{-5} M in CH_2Cl_2 (top) and evolution of the UV-vis spectrum of **Napht-1** ca. 10^{-5} M in chlorobenzene with temperature (bottom).

Table 2. UV-vis data of **Ph-1**, **Napht-1**, **Pyr-1** and reference **TPA-T-1** in CH_2Cl_2 (ca. 10^{-5} M) and as thin films.

Compound	λ_{max} [nm] CH_2Cl_2	ε [M^{-1} cm^{-1}]	λ_{max} [nm] Film	E_g^{opt} [eV]
TPA-T-1[23]	569	4.7×10^4	592	1.70
	384	1.3×10^4	391	
	303	2.6×10^4	306	
Ph-1	571	1.7×10^4	595	1.70
	391	5.0×10^3	403	
	305	1.5×10^4	310	
Napht-1	571	3.3×10^4	598	1.71
	391	1.5×10^4	400	
	336	2.7×10^4	343	
Pyr-1	580	3.3×10^4	606	1.65
	401	2.2×10^4	411	
	307	3.7×10^4	312	

Photophysics

Steady state PL measurements showed the absence of photoemission for **Ph-1**, **Napht-1** and **Pyr-1** (ca. 10^{-6} M) in dichloromethane, chloroform, toluene and hexane. Ultrafast time-resolved photoluminescence (TRPL) measurements were also performed with the excitation wavelength set at $\approx 580 \pm 10$ nm to ensure optimal light absorption and the photoexcitation of the lowest excited state. However, no PL was detected. In agreement with previous photophysical investigations on other TCBD derivatives,[21,23] all these results strongly suggest very short-lived singlet excited states in solution, which are associated with an ultrafast non-radiative deactivation for all the molecules.

Chemistry–A European Journal

Full Paper
doi.org/10.1002/chem.202002810

Chemistry Europe
European Chemical
Societies Publishing

Transient absorption

To uncover the lack of PL of the compounds in solution, transient absorption (TA) measurements using the pump-probe technique were carried out (see Supporting Information for experimental details). The steady state and transient absorption spectra in chloroform are shown in Figure 5. **Ph-1**, **Napht-1** and **Pyr-1** exhibit similar UV-vis spectra to the ones previously recorded in dichloromethane, albeit with a slightly bathochromic shift of the absorption maximum of the lowest-energy bands up to ≈ 580 nm (Figure 5a, Table 3). The excitation pump and probe wavelengths were chosen in accordance with the region of interest, that is, a central wavelength of 590 nm with a full width at half maximum (FWHM) bandwidth of 27 nm. Figures 5b–d depict the pump-probe transients consisting of an ingrowing and a decaying components. The ingrowing exponent of ≈ 0.7 ps is assigned to vibrational relaxation at the excited state. The subsequent mono-exponential decay is attributed to depopulation of the excited state in ≈ 10 ps. This short decay explains why it was not possible to detect any signal with the TRPL setup with a time resolution of 10 ps.
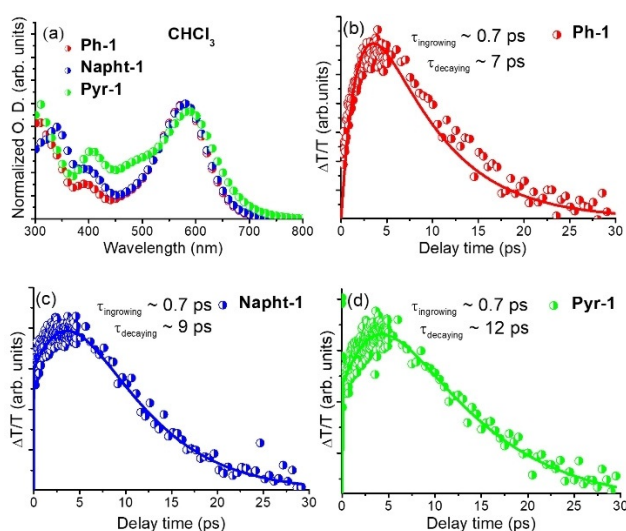
Figure 5. (a) Steady-state absorption spectra of chloroform solutions of **Ph-1** (red), **Napht-1** (blue) and **Pyr-1** (green). Transient absorption of **Ph-1** (b), **Napht-1** (c) and **Pyr-1** (d), the circles show the experimental data, while the solid lines depict the exponential fittings with respective ingrowing and decaying components. The pump and probe wavelengths for all the experiments was set at 590 nm with FWHM of 27 nm.

Table 3. Steady state absorption and PL data for titled molecules in solution, in PMMA matrix and as neat film.

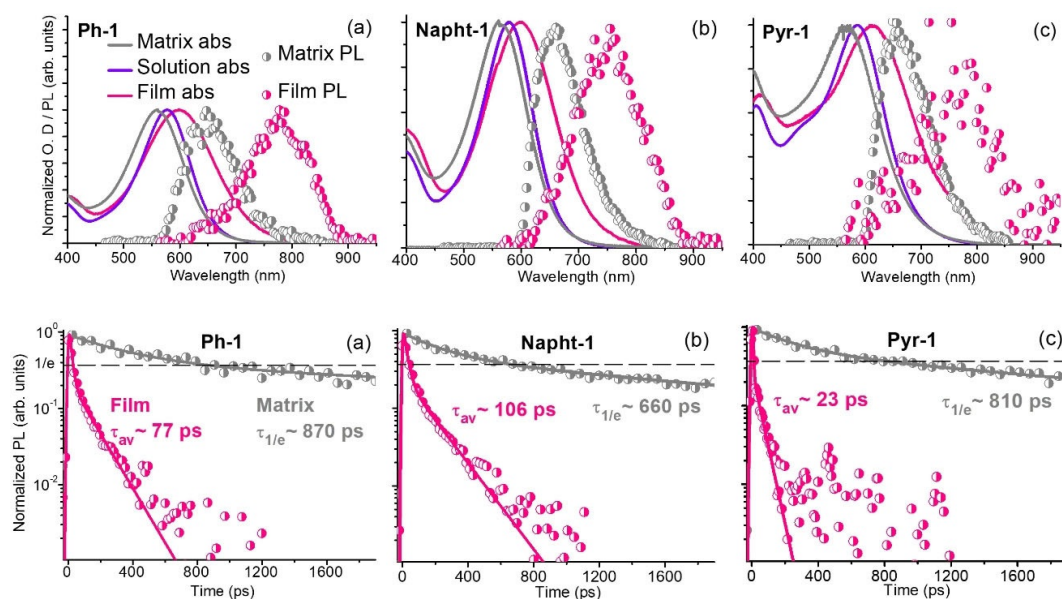| Compound	Absorption λ_{max} [nm]			Emission λ_{max} [nm]		
	CHCl$_3$	PMMA	Evap. Film	CHCl$_3$	PMMA	Evap. Film
Ph-1	577	562	598	no	653	784
Napht-1	579	566	599	no	660	757
Pyr-1	587	569	614	no	665	780

Photoluminescence dynamics of neat thin films or isolated molecules in PMMA matrices

As a next step, photophysical experiments were also performed in the solid state to assess the singlet excited state lifetime, which is of interest for photovoltaic conversion. Neat thin films of **Ph-1**, **Napht-1** and **Pyr-1** of 30 nm on quartz were prepared by evaporation process under high vacuum (ca. 10^{-6} mbar), while films of molecules dispersed in poly(methyl methacrylate) (PMMA, $M_w = 120\,000$ g mol^{-1}) were deposited on glass by solution process (see Supporting Information for more details). PMMA matrix provides an environment that restrains molecular conformational disorder (as in the neat films) but keeps the molecules well apart (as in highly diluted solutions). In this prospect, PMMA matrix is used as benchmark to interrelate solution and neat film environments.[36] Interestingly, whereas PL was not detected in solution as previously mentioned, photoexcitation into the lowest energy absorption band of **Ph-1**, **Napht-1** and **Pyr-1** either dispersed in PMMA matrices or as evaporated neat thin-films, led to photoemission. Figure 6 (top panel) shows the absorption spectra of molecules in chloroform (ca. 10^{-5} M), in PMMA matrices, in neat thin films and their respective steady state PL spectra (see also Table 3). The PL spectra were obtained by time integrating the PL maps (Figure S35) over (0–0.8) ns spectral range for the neat films and (0–1.8) ns for the PMMA matrices.

Compared to the diluted solutions in chloroform for which the target molecules can be considered as isolated, the neat films exhibit a 20–30 nm redshift of the absorption spectra due to intermolecular interactions. Molecules dispersed in the polymer matrices show a blueshifted absorption and PL spectra compared to those of the neat films suggesting the absence of intermolecular interactions.[36a] The latter is confirmed by the lack of dynamical PL mean energy shift compared to a larger shift in the neat film (see Figure S36). Compared to chloroform solutions, the absorption spectra of molecules dispersed in PMMA are even more blue-shifted (by 13–18 nm) probably due to a difference of medium polarity hence affecting the position of the ICT band.

The appearance of PL in the PMMA matrix with emission maxima between 653 and 665 nm for **Ph-1**, **Napht-1** and **Pyr-1** may be explained by a motion restriction of the molecules within the PMMA upon photoexcitation. This is also the case for neat thin-films; however due to π–π intermolecular interactions, the PL spectra are significantly shifted to lower energy, giving rise to emission with maxima at ca. 760–780 nm.

Figure 6 (bottom panel) depicts the spectra-integrated PL transients of the three molecules in PMMA matrices and neat films. The neat films PL transients have a bi-exponential behavior. The early times dynamics (< 0.1 ns) can be ascribed to a spectral relaxation or excitonic traps as evidenced from the red shift of the mean PL frequency (see Supporting Information for details), while the slowest decaying exponents should be the actual singlet exciton lifetime (see Table S3 for fitting parameters).[15,37] The singlet exciton average lifetimes in the neat films amount to 77 ps, 106 ps and 23 ps for **Ph-1**, **Napht-1** and **Pyr-1**, respectively, which are higher than the ones measured in so-

Chemistry–A European Journal

Full Paper
doi.org/10.1002/chem.202002810

Chemistry Europe
European Chemical
Societies Publishing

Figure 6. Top panel: absorption and PL spectra of (a) **Ph-1**, (b) **Napht-1** and (c) **Pyr-1**. Steady state absorption spectra of molecules isolated in PMMA matrix (gray), in chloroform (violet) and as neat thin film (pink) represented by solid lines and the corresponding time-integrated PL spectra for PMMA matrix (gray) and neat thin film (violet) represented by circles. The excitation wavelength for the PL spectra was set at $\approx 580 \pm 10$ nm. Bottom panel: Spectra-integrated (in 600–900 nm range) PL transients of (a) **Ph-1**, (b) **Napht-1** and (c) **Pyr-1** in PMMA matrices (gray circles) and neat films (pink circles) with their respective fitting (solid lines). The dash black lines represent the mean lifetime as a 1/e fraction of the maximum. The corresponding times are shown next to the transients.

lution, 7 ps, 9 ps and 12 ps, respectively (Figure 5). In addition, Figure 6 (bottom panel) shows that the singlet exciton mean lifetimes of molecules in the PMMA matrices are significantly increased up to 870 ps, 660 ps and 810 ps for **Ph-1**, **Napht-1** and **Pyr-1**, respectively. Accordingly, the occurrence of PL of **Ph-1**, **Napht-1** and **Pyr-1** in neat films and in the PMMA matrices is related to a progressive increase of singlet exciton lifetime which is extremely short in chloroform, showing also that restrained molecules in the solid state can recover their PL. A similar solid-state PL enhancement has been previously observed in other conjugated materials.[23,38]

To summarize, the combination of TRPL spectroscopy and pump-probe measurements has allowed us to gain insights into the excited state dynamics of novel TCBD-based push–pull molecules. The TA measurements revealed extremely short singlet excited state deactivation of ≈ 10 ps in solution. Using TRPL spectroscopy, we measured much longer excited state deactivation in the neat films (up to ~100 ps) and even longer times in the PMMA matrices (up to 870 ps). These altogether reveal that the confinement of the molecules in the solid state significantly limits the non-radiative losses in contrast to what is observed in solution due to molecular rearrangement upon light absorption, as discussed below.

Theoretical calculations

In order to shed some light on the absence of photoemission properties of push–pull molecules **Ph-1**, **Napht-1** and **Pyr-1** in solution, we performed a series of density functional theory (DFT) and time-dependent (TD) DFT calculations at the range-separated hybrid (RSH) ωB97X-D/6-31G(d,p) level of theory,[39]

including also a polarizable continuum model (PCM)[40] to introduce dielectric screening effects of the polarizable environment. The typical dielectric constant of chloroform $\varepsilon = 4.7$ was used to reproduce the surrounding medium. Excited-state transition energies and oscillator strengths were obtained with TDDFT calculations based on the Tamm–Dancoff approximation (TDA).[41] In particular, we computed the reorganization energy of **Napht-1** going from the optimized ground state to the fully relaxed (adiabatic) first excited state, as described in Figure 7. Values of 0.48 eV and 0.50 eV were found for λ_{S0} and λ_{S1} respectively, giving a total reorganization energy of 0.98 eV. Al-

$$\lambda_{S_0} = E(S_0|Q_1) - E(S_0|Q_0)$$
$$\lambda_{S_1} = E(S_1|Q_0) - E(S_1|Q_1)$$
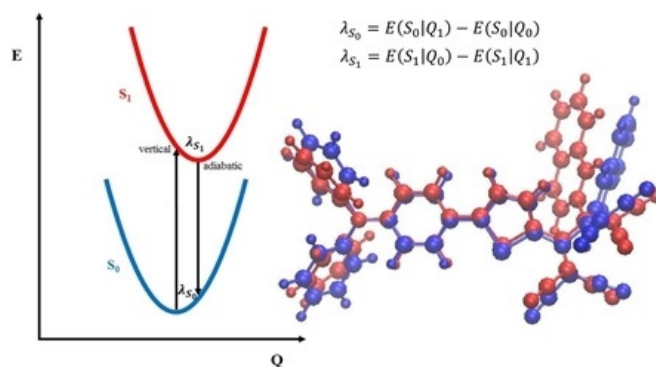
**Figure 7.** Energetic diagram and expression of the reorganization energies λ_{S1} and λ_{S0} where $E(S_m|Q_n)$ stands for the energy of the state S_m at the geometry for the state Q_n. Right: geometry of optimized the ground state of **Napht-1** (in blue) and the fully relaxed excited state (in red), generated without any constraint on the molecular soft degrees of freedom (i.e., torsion angles).

Chemistry–A European Journal

Full Paper
doi.org/10.1002/chem.202002810

Chemistry Europe
European Chemical
Societies Publishing

though the two potential energy surfaces involved are pretty much symmetrical, this large reorganization energy is ascribable to a remarkable molecular rearrangement occurring at the excited state optimized geometry.

Figure 7 shows the optimized geometry of **Napht-1** in its excited state (in red) calculated starting from the optimized ground state geometry (in blue) and without any constraint on the dihedral angles of the molecule, thus mimicking the situation in a solvent. By superimposing the nitrogen atom of the TPA unit, the comparison clearly evidences the geometrical variations occurring between both twisted ground and excited states. In particular, along with a minor rearrangement of the TPA unit, the most considerable changes take place on the TCBD and the naphthalene moieties. For instance, the initial dihedral angle of 79° between the two dicyanovinyl groups of the TCBD moiety in the ground state (77° from X-ray data) is significantly affected in the excited state leading to a smaller value of 39°. As a matter of fact, the high reorganization energy found for **Napht-1** can be correlated to these significant geometrical changes upon photoexcitation, which opens a possible efficient pathway for a non-radiative decay, thus preventing the molecule to be photoluminescent in solution.

This conformational relaxation has also some consequences on the charge transfer (CT) nature of the excited state and on the oscillator strength of the transition. In order to quantify the former, we took advantage of the spatial overlap metric Φ_S between hole and electron densities.[42] Indeed, the vertical excited state transition (Figure 8, bottom) performed on the ground-state structure shows a weaker intramolecular CT state (higher Φ_S character of 0.69 with an oscillator strength of 1.33), with the hole and the electron density delocalized on the molecular backbone. On the other hand, the fully relaxed excited state transition (Figure 8, top) turns out to yield a stronger twisted intramolecular CT state (lower Φ_S character of 0.60 with an oscillator strength of 0.76). The TCBD rearrangement upon photoexcitation electronically decouples the TPA electron-donor group from the rest of the molecule, so that the electron density resides mostly on the TCBD electron acceptor group.
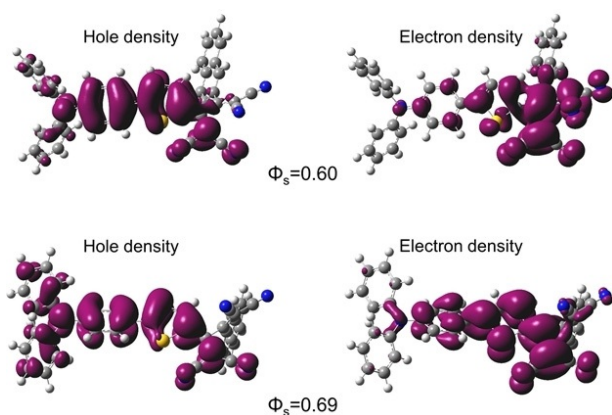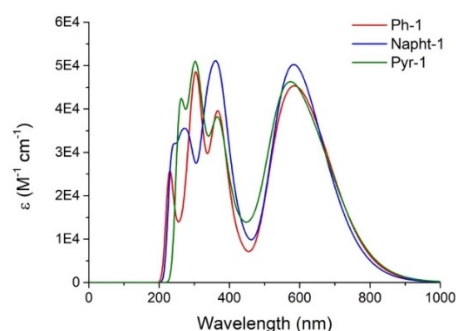
As a proxy for solid-state effects, we calculated the reorganization energy by performing a constrained relaxed excited state optimization, that is, freezing all the soft torsion angles of the molecule. By doing that, smaller relaxation energy values of 0.19 eV and 0.28 eV were found, respectively for λ_{S0} and λ_{S1}, which could explain the recovery of fluorescence when such molecules are embedded in a solid PMMA matrix. In addition, in contrast to what is obtained in the full conformational relaxation scenario mimicking the situation in solution, there is almost no significant structural variation between the ground state geometry and the constrained relaxed excited state one (Figure S39), neither in terms of CT character ($\Phi_S = 0.69$ vs. 0.72, respectively) nor for the oscillator strength (1.33 vs. 1.56, respectively).

TDA-TDDFT calculations employing an optimally tuned (OT) RSH ωB97X-D/6-31G(d,p) level of theory combined with PCM ($\varepsilon = 4.7$) were also performed to investigate the optical properties of the three TCBD-based molecules. The simulated UV-vis spectra of **Ph-1**, **Napht-1** and **Pyr-1** in chloroform are represented in Figure 9.
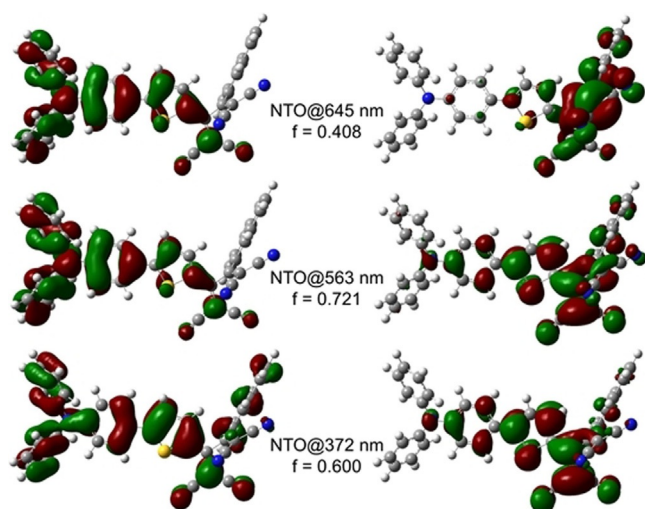
The theoretical absorption spectra are in good agreement with the experimental ones (Figure 5a). Table 4 shows the three main electronic transitions for each compound (see also Figure S40). In all cases, the calculated transition at around 650 nm is assigned to a HOMO → LUMO contribution while the transition at around 560 nm corresponds to a HOMO → LUMO + 1. Figure 10 presents the electronic excitations related to **Napht-1** depicted by Natural Transition Orbitals (NTOs). The two electronic transitions at 645 nm (HOMO → LUMO) and 563 nm (HOMO → LUMO + 1) for **Napht-1** show a strong CT character from the TPA-T moiety to TCBD, contributing both to the broad band observed experimentally at λ_{max} of 579 nm.

Figure 8. Hole and electron densities distribution, along with the charge transfer character Φ_S computed in the full relaxed (top) and vertical (bottom) excited state for **Napht-1**.

Figure 9. Calculated TDA-TDDFT absorption spectra of **Ph-1**, **Napht-1** and **Pyr-1**.

Table 4. Main calculated electronic transitions of **Ph-1**, **Napht-1**, **Pyr-1** in chloroform and their orbital description, where H and L denote HOMO and LUMO, respectively.

Compound	H−n→L+1	H→L+1	H→L
Ph-1	370 nm ($n=1$)	555 nm	648 nm
Napht-1	372 nm ($n=2$)	563 nm	645 nm
Pyr-1	371 nm ($n=2$)	556 nm	656 nm

Chemistry–A European Journal

Full Paper
doi.org/10.1002/chem.202002810

Chemistry Europe
European Chemical
Societies Publishing

Figure 10. Electronic excitations related to **Napht-1** depicted by natural transition orbitals (NTOs) for the three main transitions with oscillator strengths, hole densities are shown on the left and electron densities on the right.

The calculated peak at 372 nm attributed to a HOMO−2 → LUMO+1 transition for **Napht-1** involves the concomitant charge transfer from TPA-T and the naphthyl moiety to the TCBD acceptor. A similar behavior is observed for **Ph-1** and **Pyr-1** (Figures S41 and S42). In the case of **Pyr-1**, the calculated electronic transition at 474 nm (Figures S40 and S42), with a relatively high oscillator strength (f = 0.127), exhibits a strong Pyrene TCBD charge transfer character. We associate that transition to the shoulder observed at ca. 480 nm in the experimental absorption spectrum (Figure 5a).

Thus, photophysical experiments combined with computational studies suggest that the ultra-short relaxation of the singlet excited state of **Ph-1**, **Napht-1** and **Pyr-1** in solution (ca. 10 ps) is related to significant geometrical changes occurring at the TCBD-arene moiety upon photoexcitation causing the molecules not to be emissive. This process is hindered in the solid state, thereby leading to a recovery of PL with an enhancement of the excited state deactivation time. Though the latter remains relatively short for neat thin films with values ranging from ca. 20 up to 100 ps, they are high enough to facilitate exciton dissociation at a donor/acceptor interface in organic solar cells.[43]

Photovoltaic performance

In order to evaluate the potential of the titled compounds as electron donors for OPV, all vacuum-processed planar heterojunction (PHJ) OSCs were fabricated with the following configuration: ITO/C$_{60}$ (15 nm)/Donor (6 or 10 nm, respectively)/ BPAPF (10 nm)/BPAPF:NDP9 (45 nm, 9.5 wt%)/NDP9 (1 nm)/ Al (100 nm). BPAPF (9,9-bis[4-(N,N-bisbiphenyl-4-yl-amino)-phenyl]-9H-fluorene) and NDP9 (from Novaled) were used as hole transporting material and p-dopant, respectively. The photovoltaic parameters of these devices are gathered in Table 5. The thickness of the donor **Ph-1**, **Napht-1** or **Pyr-1** has been fixed at 6 or 10 nm to study its effect on the fill factor (FF) and

Table 5. Photovoltaic parameters of vacuum-processed PHJ OSCs ITO/ C$_{60}$/Donor/BPAPF/BPAPF:NDP9/NDP9/Al prepared from **Ph-1**, **Napht-1** and **Pyr-1** and characterized under AM 1.5 simulated solar illumination at 100 mW cm^{-2} (+/−2%).

Donor	d [nm][a]	V_{oc} [V]	J_{sc} [mA cm^{-2}]	FF [%]	PCE [%]
Ph-1	6	0.99	3.3	57	1.86
	10	0.99	3.0	55	1.63
Napht-1	6	0.98	2.3	55	1.23
	10	0.96	2.1	54	1.09
Pyr-1	6	0.97	2.1	47	0.96
	10	0.96	1.8	46	0.74

[a] Thickness.

the current density (J), which gives a first insight into recombination and charge transport behavior (Figure S43). We found that for each compound, the PCE value slightly decreased with the thickness of the donor layer owing to a decrease of the short-circuit current density (J_{sc}) suggesting poor hole transport properties of the twisted target compounds. Comparison of the photovoltaic parameters of OSCs for the different donors shows an increase of performance with the size reduction of the cyclic aromatic hydrocarbons from pyrene (PCE = 0.96%) to naphthalene (PCE = 1.23%) and benzene (PCE = 1.86%), the corresponding J vs. V curves for a donor layer of 6 nm being represented in Figure 11. Comparison of absorption spectra of 30 nm-thick evaporated thin films of **Ph-1**, **Napht-1** and **Pyr-1** on quartz (Figure S44) suggests that the best PCE value for **Ph-1** mainly results from the higher absorption of **Ph-1**, leading to a higher J_{sc} value corresponding to the slightly more intense external quantum efficiency (EQE) spectra (Figure S43).

Conventional bilayer OSCs of architecture ITO/PEDOT-PSS/ Donor/C$_{60}$/Al were also prepared by spin-coating a solution of each donor in chloroform (see Supporting Information). The same trend in terms of photovoltaic performance was observed, the higher PCE of 0.95% for **Ph-1** being associated to
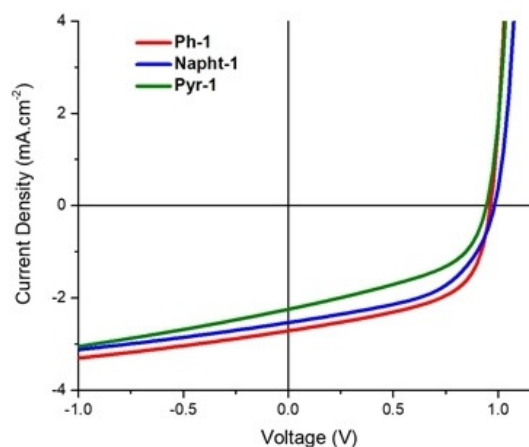
Figure 11. Comparison of the current density-voltage curves of vacuum-processed PHJ OSCs prepared from **Ph-1**, **Napht-1** and **Pyr-1** (6 nm thickness) under AM 1.5 simulated solar illumination at 100±2 mW cm^{-2}.

Chemistry–A European Journal

Full Paper
doi.org/10.1002/chem.202002810

Chemistry Europe
European Chemical
Societies Publishing

an open-circuit voltage (V_{oc}) of 0.62 V, a J_{sc} of 4.4 mA cm^{-2} and a FF of 34% (Figure S45 and Table S4). For comparison, all vacuum-processed PHJ OSCs led to better results as compared to OSCs fabricated by solution process. In addition, much higher V_{oc} values close to 1 V are obtained for vacuum-processed devices as well as increased FF values up to 57% probably resulting from the presence of additional interfaces providing better collection of charges.

Thus, compared to **Ph-1**, the introduction of larger aromatic platforms in **Napht-1** and **Pyr-1** appears detrimental for photovoltaic performance of planar heterojunction OSCs with C$_{60}$. In addition to the aforementioned optical properties of thin-films, several other hypotheses can be proposed to explain this behavior. It is known that efficient charge generation is highly dependent on the fullerene aggregate size and packing in bulk heterojunctions between polymer donor and fullerene acceptors.[44] However in the case of planar heterojunction OSCs with a fixed evaporated layer of C$_{60}$, the lower performance obtained for **Pyr-1** might be related to the lower energetic driving force for charge transfer in agreement with the smaller difference measured between its LUMO level and that of C$_{60}$. On the other hand, the shortest singlet exciton average lifetime measured for **Pyr-1** in neat film (23 ps) might induce a shorter exciton diffusion length and hence a lower exciton dissociation rate. Indeed, even the best photovoltaic performance obtained for **Ph-1** remains quite low compared to the PV performance reported for analogous push–pull molecules with a DCV electron-withdrawing unit,[8d, e, 9, 10b, c, 11, 13a, 15] one possible reason can stem from the significantly longer singlet excited state lifetimes of the later derivatives and hence their higher diffusion lengths.[15] As a consequence, TCBD-based push–pull molecules can be used as donor materials in OSCs, however their relative short singlet excited state lifetimes in the solid state, seems to limit their photovoltaic performance.

Conclusions

A series of D-π-A push–pull π-conjugated molecules based on triphenylamine as electron-donating group D, a thiophene π-spacer and tetracyanobutadiene (TCBD) as electron-withdrawing group A, and end-capped with arene platforms of increasing size from a phenyl, a 2-naphthyl or a 1-pyrenyl substituent, were synthesized in few steps and in good yields. The synthesis was optimized thanks to the use of an efficient Seyferth–Gilbert homologation of a conjugated aldehyde affording a free conjugated alkyne derivative, which was subject to a selective copper-free Sonogashira reaction with halogenoarenes in order to avoid Glaser homocouplings. Finally, a [2+2] cycloaddition-retroelectrocyclization reaction between the unsymmetrical electron-rich alkynes and tetracyanoethylene quantitatively led to the target molecules **Ph-1**, **Napht-1** and **Pyr-1**.

As shown by X-ray diffraction analysis of single crystals of **Napht-1**, the highly twisted TCBD moiety limits π–π intermolecular interactions, although short S⋯S intermolecular distances have been observed. While the target molecules show typical electrochemical oxidation behavior of triphenylamine derivatives, they can also be reversibly reduced at accessible negative potentials in agreement with the strong electron-withdrawing character of TCBD, which is exalted when it is conjugated with the pyrene unit. They also exhibit good absorption in the visible range due to their inherent ICT band. Moreover, they present frontier orbitals compatible with their use as donor materials for organic solar cells in combination with C$_{60}$.

Photophysical experiments showed that the molecules exhibited extremely fast depopulation of their singlet excited state in solution (≈ 10 ps), preventing them to be photoemissive. As supported by theoretical calculations, these values can be explained by the high reorganization energy of the molecules upon photoexcitation associated with significant conformational changes of the TCBD-arene moiety. Interestingly, the singlet excited state deactivation time decay for all the compounds progressively increases (by two orders of magnitude) from the solution to the neat thin films and then in the PMMA matrices, respectively, leading to a recovery of PL. This behavior results from a restriction of structural disorder, which is of interest for photovoltaic conversion. Hence, we prepared all vacuum-processed planar heterojunction organic solar cells with a power conversion efficiency of ca. 1.9% for **Ph-1** whereas a decrease of photovoltaic performance was observed with the increase of the arene size.

Our findings not only disentangle the underlying factors behind the lack of photoemission in solution, but also offer structural, photophysical and theoretical insights into these TCBD push–pull molecules for potential use in organic semiconductors devices. For instance, the design of more π-extended TCBD-based conjugated systems with reduced conformational changes upon photoexcitation could be of interest for novel donor or non-fullerene acceptor materials for organic photovoltaics.

Experimental Section

Crystallographic data

Deposition number 1994639 (**Napht-1**) contains the supplementary crystallographic data for this paper. These data are provided free of charge by the joint Cambridge Crystallographic Data Centre and Fachinformationszentrum Karlsruhe Access Structures service.

Acknowledgements

Conflict of interest

The authors declare no conflict of interest.

[1] L. R. Dalton, P. A. Sullivan, D. H. Bale, *Chem. Rev.* **2010**, *110*, 25–55.

[2] a) J. M. Raimundo, P. Blanchard, N. Gallego-Planas, N. Mercier, I. Ledoux-Rak, R. Hierle, J. Roncali, *J. Org. Chem.* **2002**, *67*, 205–218; b) J. D. Luo, X. H. Zhou, A. K. Y. Jen, *J. Mater. Chem.* **2009**, *19*, 7410–7424; c) C. Cabanetos, W. Bentoumi, V. Silvestre, E. Blart, Y. Pellegrin, V. Montembault, A. Barsella, K. Dorkenoo, Y. Bretonnière, C. Andraud, L. Mager, L. Fontaine, F. Odobel, *Chem. Mater.* **2012**, *24*, 1143–1157; d) A. B. Marco, N. Martinez de Baroja, S. Franco, J. Garin, J. Orduna, B. Villacampa, A. Revuelto, R. Andreu, *Chem. Asian J.* **2015**, *10*, 188–197.

[3] a) C.-T. Chen, *Chem. Mater.* **2004**, *16*, 4389–4400; b) H. Uoyama, K. Goushi, K. Shizu, H. Nomura, C. Adachi, *Nature* **2012**, *492*, 234–238; c) L. Yao, S. Zhang, R. Wang, W. Li, F. Shen, B. Yang, Y. Ma, *Angew. Chem. Int. Ed.* **2014**, *53*, 2119–2123; *Angew. Chem.* **2014**, *126*, 2151–2155; d) D. H. Kim, A. D'Aléo, X. K. Chen, A. D. S. Sandanayaka, D. D. Yao, L. Zhao, T. Komino, E. Zaborova, G. Canard, Y. Tsuchiya, E. Choi, J. W. Wu, F. Fages, J. L. Brédas, J. C. Ribierre, C. Adachi, *Nat. Photonics* **2018**, *12*, 98–106; e) Y. C. Liu, C. S. Li, Z. J. Ren, S. K. Yan, M. R. Bryce, *Nat. Rev. Mater.* **2018**, *3*, 18020; f) W. W. H. Lee, Z. Zhao, Y. Cai, Z. Xu, Y. Yu, Y. Xiong, R. T. K. Kwok, Y. Chen, N. L. C. Leung, D. Ma, J. W. Y. Lam, A. Qin, B. Z. Tang, *Chem. Sci.* **2018**, *9*, 6118–6125; g) W. Zeng, T. Zhou, W. Ning, C. Zhong, J. He, S. Gong, G. Xie, C. Yang, *Adv. Mater.* **2019**, *31*, 1901404.

[4] a) E. Genin, Z. Gao, J. A. Varela, J. Daniel, T. Bsaibess, I. Gosse, L. Groc, L. Cognet, M. Blanchard-Desce, *Adv. Mater.* **2014**, *26*, 2258–2261; b) E. Campioli, D. M. Nikolaidou, V. Hugues, M. Campanini, L. Nasi, M. Blanchard-Desce, F. Terenziani, *J. Mater. Chem. C* **2015**, *3*, 7483–7491; c) X. Yan, M. Remond, Z. Zheng, E. Hoibian, C. Soulage, S. Chambert, C. Andraud, B. Van der Sanden, F. Ganachaud, Y. Bretonnière, J. Bernard, *ACS Appl. Mater. Interfaces* **2018**, *10*, 25154–25165; d) M. Rémond, Z. Zheng, E. Jeanneau, C. Andraud, Y. Bretonnière, S. Redon, *J. Org. Chem.* **2019**, *84*, 9965–9974; e) A. H. Ashoka, P. Ashokkumar, Y. P. Kovtun, A. S. Klymchenko, *J. Phys. Chem. Lett.* **2019**, *10*, 2414–2421.

[5] B. E. Hardin, H. J. Snaith, M. D. McGehee, *Nat. Photonics* **2012**, *6*, 162–169.

[6] T. D. Kim, K. S. Lee, *Macromol. Rapid Commun.* **2015**, *36*, 943–958.

[7] Y. Shirota, H. Kageyama, *Chem. Rev.* **2007**, *107*, 953–1010.

[8] a) J. Roncali, P. Leriche, P. Blanchard, *Adv. Mater.* **2014**, *26*, 3821–3838; b) V. Malytskyi, J.-J. Simon, L. Patrone, J.-M. Raimundo, *RSC Adv.* **2015**, *5*, 354–397; c) J. Wang, K. Liu, L. Ma, X. Zhan, *Chem. Rev.* **2016**, *116*, 14675–14725; d) P. Blanchard, C. Malacrida, C. Cabanetos, J. Roncali, S. Ludwigs, *Polym. Int.* **2019**, *68*, 589–606; e) C. Cabanetos, P. Blanchard, J. Roncali, *Chem. Rec.* **2019**, *19*, 1123–1130.

[9] a) N. Cho, S. Paek, J. Jeon, K. Song, G. D. Sharma, J. Ko, *J. Mater. Chem. A* **2014**, *2*, 12368–12379; b) J. Min, Y. N. Luponosov, D. Baran, S. N. Chvalun, M. A. Shcherbina, A. V. Bakirov, P. V. Dmitryakov, S. M. Peregudova, N. Kausch-Busies, S. A. Ponomarenko, T. Ameri, C. J. Brabec, *J. Mater. Chem. A* **2014**, *2*, 16135–16147; c) A. Mishra, C. Wetzel, R. Singhal, P. Bäuerle, G. D. Sharma, *J. Phys. Chem. C* **2018**, *122*, 11262–11269.

[10] a) V. Steinmann, N. M. Kronenberg, M. R. Lenze, S. M. Graf, D. Hertel, K. Meerholz, H. Burckstummer, E. V. Tulyakova, F. Würthner, *Adv. Energy Mater.* **2011**, *1*, 888–893; b) S. W. Chiu, L. Y. Lin, H. W. Lin, Y. H. Chen, Z. Y. Huang, Y. T. Lin, F. Lin, Y. H. Liu, K. T. Wong, *Chem. Commun.* **2012**, *48*, 1857–1859; c) Y. H. Chen, L. Y. Lin, C. W. Lu, F. Lin, Z. Y. Huang, H. W. Lin, P. H. Wang, Y. H. Liu, K. T. Wong, J. Wen, D. J. Miller, S. B. Darling, *J. Am. Chem. Soc.* **2012**, *134*, 13616–13623; d) X. Z. Che, C.-L. Chung, C.-C. Hsu, F. Liu, K.-T. Wong, S. R. Forrest, *Adv. Energy Mater.* **2018**, *8*, 1703603.

[11] a) X. Z. Che, X. Xiao, J. D. Zimmerman, D. J. Fan, S. R. Forrest, *Adv. Energy Mater.* **2014**, *4*, 1400568; b) X. Z. Che, Y. X. Li, Y. Qu, S. R. Forrest, *Nat. Energy* **2018**, *3*, 422–427.

[12] S. Roquet, A. Cravino, P. Leriche, O. Alévêque, P. Frère, J. Roncali, *J. Am. Chem. Soc.* **2006**, *128*, 3459–3466.

[13] a) A. Leliège, C. H. Le Régent, M. Allain, P. Blanchard, J. Roncali, *Chem. Commun.* **2012**, *48*, 8907–8909; b) A. Leliège, J. Grolleau, M. Allain, P. Blanchard, D. Demeter, T. Rousseau, J. Roncali, *Chem. Eur. J.* **2013**, *19*, 9948–9960; c) J. W. Choi, C. H. Kim, J. Pison, A. Oyedele, D. Tondelier, A. Leliège, E. Kirchner, P. Blanchard, J. Roncali, B. Geffroy, *RSC Adv.* **2014**, *4*, 5236–5242; d) A. Labrunie, Y. Jiang, F. Baert, A. Leliège, J. Roncali, C. Cabanetos, P. Blanchard, *RSC Adv.* **2015**, *5*, 102550–102554.

[14] a) Y. Jiang, C. Cabanetos, M. Allain, P. Liu, J. Roncali, *J. Mater. Chem. C* **2015**, *3*, 5145–5151; b) S. Mohamed, D. Demeter, J. A. Laffitte, P. Blanchard, J. Roncali, *Sci. Rep.* **2015**, *5*, 9031; c) Y. Jiang, C. Cabanetos, S. Jungsuttiwong, D. Alberga, C. Adamo, J. Roncali, *ChemistrySelect* **2017**, *2*, 6296–6303.

[15] O. V. Kozlov, Y. N. Luponosov, A. N. Solodukhin, B. Flament, O. Douheret, P. Viville, D. Beljonne, R. Lazzaroni, J. Cornil, S. A. Ponomarenko, M. S. Pshenichnikov, *Org. Electron.* **2018**, *53*, 185–190.

[16] a) S. Kato, F. Diederich, *Chem. Commun.* **2010**, *46*, 1994–2006; b) T. Michinobu, F. Diederich, *Angew. Chem. Int. Ed.* **2018**, *57*, 3552–3577; *Angew. Chem.* **2018**, *130*, 3612–3638.

[17] a) X. M. Wu, J. Y. Wu, Y. Q. Liu, A. K. Y. Jen, *J. Am. Chem. Soc.* **1999**, *121*, 472–473; b) C. Cai, I. Liakatas, M.-S. Wong, M. Bösch, C. Bosshard, P. Günter, S. Concilio, N. Tirelli, U. W. Suter, *Org. Lett.* **1999**, *1*, 1847–1849; c) T. Michinobu, J. C. May, J. H. Lim, C. Boudon, J. P. Gisselbrecht, P. Seiler, M. Gross, I. Biaggio, F. Diederich, *Chem. Commun.* **2005**, 737–739.

[18] S. Kato, M. Kivala, W. B. Schweizer, C. Boudon, J. P. Gisselbrecht, F. Diederich, *Chem. Eur. J.* **2009**, *15*, 8687–8691.

[19] a) S. Niu, G. Ulrich, P. Retailleau, R. Ziessel, *Org. Lett.* **2011**, *13*, 4996–4999; b) P. Gautam, R. Misra, M. B. Thomas, F. D'Souza, *Chem. Eur. J.* **2017**, *23*, 9192–9200; c) R. García, M. A. Herranz, M. R. Torres, P. A. Bouit, J. L. Delgado, J. Calbo, P. M. Viruela, E. Orti, N. Martin, *J. Org. Chem.* **2012**, *77*, 10707–10717; d) F. Tancini, F. Monti, K. Howes, A. Belbakra, A. Listorti, W. B. Schweizer, P. Reutenauer, J. L. Alonso-Gomez, C. Chiorboli, L. M. Urner, J. P. Gisselbrecht, C. Boudon, N. Armaroli, F. Diederich, *Chem. Eur. J.* **2014**, *20*, 202–216; e) C. Dengiz, B. Breiten, J. P. Gisselbrecht, C. Boudon, N. Trapp, W. B. Schweizer, F. Diederich, *J. Org. Chem.* **2015**, *80*, 882–896; f) M. Sekita, B. Ballesteros, F. Diederich, D. M. Guldi, G. Bottari, T. Torres, *Angew. Chem. Int. Ed.* **2016**, *55*, 5560–5564; *Angew. Chem.* **2016**, *128*, 5650–5654; g) K. A. Winterfeld, G. Lavarda, J. Guilleme, M. Sekita, D. M. Guldi, T. Torres, G. Bottari, *J. Am. Chem. Soc.* **2017**, *139*, 5520–5529; h) T. Shoji, S. Ito, *Chem. Eur. J.* **2017**, *23*, 16696–16709; i) R. Garcia, J. Calbo, R. Viruela, M. A. Herranz, E. Orti, N. Martin, *ChemPlusChem* **2018**, *83*, 300–307; j) P. Srinivasa Rao, A. L. Puyad, S. V. Bhosale, S. V. Bhosale, *Int. J. Mol. Sci.* **2019**, *20*, 1621.

[20] C. Koos, P. Vorreau, T. Vallaitis, P. Dumon, W. Bogaerts, R. Baets, B. Esembeson, I. Biaggio, T. Michinobu, F. Diederich, W. Freude, J. Leuthold, *Nat. Photonics* **2009**, *3*, 216–219.

[21] F. Monti, A. Venturini, A. Nenov, F. Tancini, A. D. Finke, F. Diederich, N. Armaroli, *J. Phys. Chem. A* **2015**, *119*, 10677–10683.

[22] J. Xu, X. Liu, J. Lv, M. Zhu, C. Huang, W. Zhou, X. Yin, H. Liu, Y. Li, J. Ye, *Langmuir* **2008**, *24*, 4231–4237.

[23] A. T. Bui, C. Philippe, M. Beau, N. Richy, M. Cordier, T. Roisnel, L. Lemiegre, O. Mongin, F. Paul, Y. Trolez, *Chem. Commun.* **2020**, *56*, 3571–3574.

[24] A. Leliège, P. Blanchard, T. Rousseau, J. Roncali, *Org. Lett.* **2011**, *13*, 3098–3101.

[25] a) P. Gautam, R. Misra, E. N. Koukaras, A. Sharma, G. D. Sharma, *Org. Electron.* **2015**, *27*, 72–83; b) P. Gautam, R. Misra, S. A. Siddiqui, G. D. Sharma, *Org. Electron.* **2015**, *19*, 76–82; c) P. Gautam, R. Misra, S. A. Siddiqui, G. D. Sharma, *ACS Appl. Mater. Interfaces* **2015**, *7*, 10283–10292; d) P. Gautam, R. Misra, G. D. Sharma, *Phys. Chem. Chem. Phys.* **2016**, *18*, 7235–7241; e) A. A. Raheem, S. Kamaraj, V. Sannasi, C. Praveen, *Org. Chem. Front.* **2018**, *5*, 777–787.

[26] a) Y. Patil, R. Misra, M. L. Keshtov, G. D. Sharma, *J. Phys. Chem. C* **2016**, *120*, 6324–6335; b) P. Srinivasa Rao, A. Gupta, S. V. Bhosale, A. Bilic, W. Xiang, R. A. Evans, S. V. Bhosale, *Dyes Pigm.* **2017**, *146*, 502–511; c) Y. Patil, R. Misra, R. Singhal, G. D. Sharma, *J. Mater. Chem. A* **2017**, *5*, 13625–13633; d) Y. Patil, R. Misra, M. L. Keshtov, G. D. Sharma, *J. Mater. Chem. A* **2017**, *5*, 3311–3319; e) P. Gautam, R. Sharma, R. Misra, M. L.

Keshtov, S. A. Kuklin, G. D. Sharma, *Chem. Sci.* **2017**, *8*, 2017–2024; f) Y. Patil, R. Misra, *Chem. Asian J.* **2018**, *13*, 220–229.

[27] Z. Pokladek, N. Ripoche, M. Betou, Y. Trolez, O. Mongin, J. Olesiak-Banska, K. Matczyszyn, M. Samoc, M. G. Humphrey, M. Blanchard-Desce, F. Paul, *Chem. Eur. J.* **2016**, *22*, 10155–10167.

[28] a) B. Dhokale, T. Jadhav, S. M. Mobin, R. Misra, *RSC Adv.* **2015**, *5*, 57692–57699; b) W. Jiang, Y. Shen, Y. Ge, C. Zhou, Y. Wen, H. Liu, S. Zhang, P. Lu, B. Yang, *J. Mater. Chem. C* **2020**, *8*, 3367–3373.

[29] O. P. Lee, A. T. Yiu, P. M. Beaujuge, C. H. Woo, T. W. Holcombe, J. E. Millstone, J. D. Douglas, M. S. Chen, J. M. Fréchet, *Adv. Mater.* **2011**, *23*, 5359–5363.

[30] A. Labrunie, J. Gorenflot, M. Babics, O. Alévêque, S. Dabos-Seignon, A. H. Balawi, Z. Kan, M. Wohlfahrt, E. Levillain, P. Hudhomme, P. M. Beaujuge, F. Laquai, C. Cabanetos, P. Blanchard, *Chem. Mater.* **2018**, *30*, 3474–3485.

[31] a) H. Huang, H. Liu, H. Jiang, K. Chen, *J. Org. Chem.* **2008**, *73*, 6037–6040; b) M. E. Ragoussi, G. de la Torre, T. Torres, *Eur. J. Org. Chem.* **2013**, 2832–2840; c) R. Chinchilla, C. Najera, *Chem. Rev.* **2007**, *107*, 874–922.

[32] a) R. Fitzner, E. Reinold, A. Mishra, E. Mena-Osteritz, H. Ziehlke, C. Korner, K. Leo, M. Riede, M. Weil, O. Tsaryova, A. Weiss, C. Uhrich, M. Pfeiffer, P. Bäuerle, *Adv. Funct. Mater.* **2011**, *21*, 897–910; b) R. Fitzner, C. Elschner, M. Weil, C. Uhrich, C. Korner, M. Riede, K. Leo, M. Pfeiffer, E. Reinold, E. Mena-Osteritz, P. Bäuerle, *Adv. Mater.* **2012**, *24*, 675–680.

[33] a) D. Cortizo-Lacalle, A. Pertegas, L. Martinez-Sarti, M. Melle-Franco, H. J. Bolink, A. Mateo-Alonso, *J. Mater. Chem. C* **2015**, *3*, 9170–9174; b) J. Li, S. Chen, P. Zhang, Z. Wang, G. Long, R. Ganguly, Y. Li, Q. Zhang, *Chem. Asian J.* **2016**, *11*, 136–140.

[34] C. M. Cardona, W. Li, A. E. Kaifer, D. Stockdale, G. C. Bazan, *Adv. Mater.* **2011**, *23*, 2367–2371.

[35] Q. Xie, E. Perez-Cordero, L. Echegoyen, *J. Am. Chem. Soc.* **1992**, *114*, 3978–3980.

[36] a) E. Salamatova, O. V. Kozlov, Y. N. Luponosov, A. N. Solodukhin, V. Y. Toropynina, S. A. Ponomarenko, M. S. Pshenichnikov, *Visualization of Molecular Excitons Diffusion*, Proc. SPIE 9923, Physical Chemistry of Interfaces and Nanomaterials XV, 99230K (26 September 2016); https://doi.org/10.1117/12.2237620; b) O. V. Kozlov, Y. N. Luponosov, A. N. Solodukhin, B. Flament, Y. Olivier, R. Lazzaroni, J. Cornil, S. A. Ponomarenko, M. S. Pshenichnikov, *Adv. Opt. Mater.* **2017**, *5*, 1700024.

[37] O. V. Mikhnenko, M. Kuik, J. Lin, N. van der Kaap, T. Q. Nguyen, P. W. Blom, *Adv. Mater.* **2014**, *26*, 1912–1917.

[38] J. Shi, L. E. Aguilar Suarez, S.-J. Yoon, S. Varghese, C. Serpa, S. Y. Park, L. Lüer, D. Roca-Sanjuán, B. Milián-Medina, J. Gierschner, *J. Phys. Chem. C* **2017**, *121*, 23166–23183.

[39] Y. S. Lin, G. D. Li, S. P. Mao, J. D. Chai, *J. Chem. Theory Comput.* **2013**, *9*, 263–272.

[40] J. Tomasi, B. Mennucci, R. Cammi, *Chem. Rev.* **2005**, *105*, 2999–3093.

[41] S. Hirata, M. Head-Gordon, *Chem. Phys. Lett.* **1999**, *314*, 291–299.

[42] G. Londi, R. Dilmurat, G. D'Avino, V. Lemaur, Y. Olivier, D. Beljonne, *Phys. Chem. Chem. Phys.* **2019**, *21*, 25023–25034.

[43] a) N. S. Sariciftci, L. Smilowitz, A. J. Heeger, F. Wudl, *Science* **1992**, *258*, 1474–1476; b) I. A. Howard, F. Laquai, *Macromol. Chem. Phys.* **2010**, *211*, 2063–2070.

[44] A. C. Jakowetz, M. L. Bohm, J. Zhang, A. Sadhanala, S. Huettner, A. A. Bakulin, A. Rao, R. H. Friend, *J. Am. Chem. Soc.* **2016**, *138*, 11672–11679.